

Article

Rate-Splitting-Based Generalized Multiple Access for Band-Limited Multi-User VLC

Yuru Tang ¹, Chen Chen ^{1,*} , Min Liu ¹, Pengfei Du ² and H. Y. Fu ³ 

¹ School of Microelectronics and Communication Engineering, Chongqing University, Chongqing 400044, China

² A*STAR's Singapore Institute of Manufacturing Technology, Singapore 138634, Singapore

³ Tsinghua Shenzhen International Graduate School and Tsinghua-Berkeley Shenzhen Institute, Tsinghua University, Shenzhen 518055, China

* Correspondence: c.chen@cqu.edu.cn

Abstract: In this paper, we propose a rate-splitting-based generalized multiple access (GMA) scheme for band-limited multi-user visible light communication (VLC) systems. By splitting and transmitting the input data of each user in a joint orthogonal multiple access (OMA) and non-orthogonal multiple access (NOMA) manner, the proposed rate-splitting-based GMA scheme can obtain better bandwidth utilization than OMA and suffer less severe interference than NOMA. In order to achieve the maximum sum rate over typical low-pass VLC channels, the optimal rate-splitting-based GMA scheme was first obtained through theoretical analysis and computer simulations. Subsequently, the superiority of the optimal rate-splitting-based GMA scheme over both OMA and NOMA under various channel conditions, user separations, and error propagation levels was further verified by the theoretical, simulation, and experimental results. In particular, the experimental results showed that, when the error propagation ratio was increased from 0 to 0.2, the sum rate reduction ratio was significantly reduced from 31.4% to 7.5% by replacing NOMA with the obtained optimal rate-splitting-based GMA.

Keywords: visible light communication; rate splitting; generalized multiple access



Citation: Tang, Y.; Chen, C.; Liu, M.; Du, P.; Fu, H.Y. Rate-Splitting-Based Generalized Multiple Access for Band-Limited Multi-User VLC. *Photonics* **2023**, *10*, 446. <https://doi.org/10.3390/photonics10040446>

Received: 2 March 2023

Revised: 9 April 2023

Accepted: 12 April 2023

Published: 13 April 2023



Copyright: © 2023 by the authors. Licensee MDPI, Basel, Switzerland. This article is an open access article distributed under the terms and conditions of the Creative Commons Attribution (CC BY) license (<https://creativecommons.org/licenses/by/4.0/>).

1. Introduction

Recently, the emergence of applications such as ultra-high-definition video streaming, virtual reality, and online video gaming has been rapidly driving the demand for high-speed and large-capacity wireless connectivity [1]. Considering the radio frequency (RF) spectrum congestion, traditional RF-based wireless communications may struggle to support the ever-increasing high data traffic in the near future [2]. To alleviate the RF spectrum congestion, visible light communication (VLC), possessing a huge spectrum ranging from about 380 to 780 nm, has been lately envisioned as a potential candidate to efficiently offload heavy traffic loads from the congested RF wireless networks [3]. Due to the wide adoption of light-emitting diodes (LEDs) for pervasive illumination in both indoor and outdoor environments, VLC relying on LEDs can fulfill the dual-function of illumination and communication, which has been generally viewed as one of the key enabling technologies for the Sixth-Generation (6G) mobile networks [4] and the Internet of Things (IoT) systems [5].

In a practical VLC system, there might be multiple users located within its serving coverage, and the LED access point (AP) should be able to simultaneously transmit data to all the connected users [6]. As a result, it is of practical significance to design a suitable multiple access scheme for multi-user VLC systems [7]. Moreover, practical VLC systems are generally band-limited and exhibit a typical low-pass frequency response, which is mainly due to the inherent low-pass nature of the illumination LEDs [8]. Therefore, it is also

very important to take the low-pass frequency response into consideration when designing the multiple access scheme for practical band-limited multi-user VLC systems.

1.1. Related Work and Motivation

Thus far, various multiple access schemes have already been proposed and investigated to support multiple users in VLC systems, which can be generally divided into the following three categories.

1.1.1. Orthogonal Multiple Access

When using orthogonal multiple access (OMA) in multi-user VLC systems, users are allocated with orthogonal resources such as time slots, frequency bands/subcarriers, and codewords [6]. As a result, the mutual interference between different users can be negligible in OMA-based multi-user VLC systems. In [9], time division multiple access (TDMA) was introduced for multi-user VLC systems, where the time and power allocation was optimized to maximize the downlink spectral efficiency. In [10,11], orthogonal frequency division multiple access (OFDMA) was adopted to serve multiple users in the VLC system through subcarrier allocation. In [12,13], code division multiple access (CDMA) was utilized in the VLC system where different users were allocated with orthogonal codewords to mitigate multi-user interference. Nevertheless, the mitigation of mutual interference between different users in OMA-based systems is due to the partitioning of the overall time/frequency/code resource, and as a consequence, the available resource of each user after partitioning becomes very limited.

1.1.2. Non-Orthogonal Multiple Access

To address the inefficient resource utilization issue of conventional OMA schemes, the concept of non-orthogonal multiple access (NOMA) has been proposed and introduced into VLC systems [14]. In NOMA-based multi-user VLC systems, multiple users can utilize the same time and frequency resources simultaneously by performing power-domain superposition coding (SPC) at the transmitter side and successive interference cancellation (SIC) at the receiver side [15]. By adopting constellation partitioning coding [16], joint transceiver optimization [17], or machine learning-based signal demodulation [18], the performance of NOMA-based multi-user VLC systems can be further enhanced. Moreover, NOMA can also be applied to realize energy-efficient light-fidelity (LiFi)-enabled bidirectional IoT communication [19]. Compared with OMA, the resource utilization efficiency of NOMA is significantly improved at the cost of non-negligible inter-user interference (IUI). Considering the decoding complexity, time delay, and interference level, it is generally feasible to multiplex a pair of users in the power domain sharing the same time and frequency resources [20]. In order to support more than two users in the VLC system, hybrid OFDMA/NOMA can be applied by dividing all the users into multiple user pairs. For example, a bidirectional hybrid OFDMA-/NOMA-based VLC system was experimentally demonstrated in [21], and a fairness-aware hybrid NOMA/OFDMA scheme has been further proposed for band-limited multi-user VLC systems [22]. Moreover, NOMA can also be applied in multiple-input, multiple-output (MIMO)-based multi-user VLC systems. Specifically, an indoor MIMO-NOMA-based VLC system was investigated in [23], and a hybrid three-dimensional multiple access (3DMA) scheme combining NOMA and space division multiple access (SDMA) was further introduced for multi-user MIMO-VLC systems in [24].

1.1.3. Rate-Splitting Multiple Access

Besides OMA and NOMA, rate-splitting multiple access (RSMA) has also been applied to support multiple users in multiple-input, single-output (MISO)-based VLC systems [25]. In a two-user MISO-VLC system using RSMA, the intended message for each user is first split into two parts: one is the private part, and the other is the common part. Then, two common parts of two users are multiplexed and transmitted together, while two private

parts of two users are transmitted individually [26]. In order to reduce IUI, transmitter-side precoding is generally performed in RSMA-based MISO-VLC systems [27]. It has been shown that RSMA can outperform both NOMA and SDMA in MISO-VLC systems, which can be seen as a generalized version of NOMA and SDMA, with NOMA and SDMA being its special cases [25].

1.1.4. Summary

As discussed above, both OMA and NOMA can be applied in general single-LED VLC systems, while RSMA is mainly applicable to MISO-VLC systems with at least two LEDs. As a result, RSMA cannot be directly introduced in general single-LED VLC systems. Furthermore, by comparing OMA and NOMA, we can see that OMA exhibits negligible IUI under the condition of reduced available resources for each user, while NOMA ensures an improved resource utilization efficiency, but suffering from non-negligible IUI. Clearly, OMA and NOMA stand for two extreme cases in terms of both resource utilization and IUI, and we might want to know whether a generalized version of OMA and NOMA can be designed to achieve a trade-off between resource utilization and IUI for practical band-limited multi-user single-LED VLC systems.

1.2. Main Contributions

Inspired by the concept of partial NOMA in [28], in this paper, we propose and evaluate a rate-splitting-based generalized multiple access (GMA) scheme for practical band-limited multi-user single-LED VLC systems. The main contributions of this work are summarized as follows:

- Proposal of a rate-splitting-based GMA scheme for band-limited multi-user VLC systems, which can be seen as a generalized version of OFDMA and NOMA;
- Derivation of the theoretical achievable rate of a general band-limited two-user VLC system applying rate-splitting-based GMA under the impact of both the LED's low-pass frequency response and the imperfect SIC-induced error propagation;
- Optimization of the rate-splitting-based GMA scheme to maximize the overall achievable rate of the band-limited two-user VLC system;
- Evaluation of the obtained optimal rate-splitting-based GMA scheme and other benchmark schemes in a practical band-limited two-user VLC system through extensive computer simulations and hardware experiments.

The remainder of this paper is organized as follows. Section 2 introduces the detailed system model. The comprehensive theoretical, simulation, and experimental results are presented and discussed in Section 3. Finally, Section 4 concludes the paper.

2. System Model

In this section, the channel model of a general band-limited multi-user VLC system using orthogonal frequency division multiplexing (OFDM) modulation is described firstly. Then, the principle of the proposed rate-splitting-based GMA scheme is introduced. Finally, the theoretical achievable rate of a general band-limited two-user VLC system applying rate-splitting-based GMA is derived. For the sake of clarity, Tables 1 and 2, respectively, give the lists of the variables and acronyms adopted in the following descriptions.

Table 1. The list of variables.

Variable	Definition
A	Active area of the PD
B	Signal bandwidth
d_k	Distance between the LED and the PD of the k -th user
$h_k(0)$	DC channel gain between the LED and the k -th user
$h_k(i)$	Amplitude attenuation coefficient at the i -th subcarrier of the k -th user
$g(\phi_k)$	Gain of the optical lens
m	Order of Lambertian emission
N_0	PSD of the AWGN
$n_k(i)$	Additive noise at the i -th subcarrier of the k -th user
r	Refractive index of the optical lens
S_k	Set of subcarriers allocated to the k -th user
$T(\phi_k)$	Gain of the optical filter
$x(i)$	Transmitted electrical signal at the i -th subcarrier
$y_k(i)$	Received electrical signal at the i -th subcarrier of the k -th user
ψ_k	Emission angle from the LED to the k -th user
ϕ_k	Incident angle from the LED to the k -th user
Ψ	Semi-angle at half power of the LED
Φ	Half-angle field-of-view (FOV) of the optical lens
ρ	PD responsivity

Table 2. The list of acronyms.

Acronym	Definition
AWGN	Additive white Gaussian noise
CDMA	Code division multiple access
FOV	Field-of-view
GMA	Generalized multiple access
IoT	Internet of Things
IUI	Inter-user interference
LED	Light-emitting diode
LOS	Line-of-sight
MIMO	Multiple-input, multiple-output
MISO	Multiple-input, single-output
NLOS	Non-line-of-sight
NOMA	Non-orthogonal multiple access
OFDM	Orthogonal frequency division multiplexing
OFDMA	Orthogonal frequency division multiple access
OMA	Orthogonal multiple access
PSD	Power spectral density
RF	Radio frequency
RSMA	Rate-splitting multiple access
SDMA	Space-division multiple access
SIC	Successive interference cancellation
SPC	Superposition coding
TDMA	Time division multiple access
VLC	Visible light communication

2.1. Channel Model

In a general band-limited K -user VLC system using OFDM modulation, the received electrical signal by the k -th user at the i -th subcarrier can be given by

$$y_k(i) = h_k(0)h_k(i)x(i) + n_k(i), \quad k = 1, 2, \dots, K, \quad (1)$$

where $h_k(0)$ represents the direct current (DC) channel gain between the LED and the k -th user, which is caused by the propagation of light over the spatial channel; $h_k(i)$ denotes the amplitude attenuation coefficient at the i -th subcarrier, which is mainly due to the low-pass frequency response of the LED [29], $i \in S_k$ with S_k being the set of subcarriers allocated to the k -th user; $x(i)$ is the transmitted electrical signal at the i -th subcarrier, and $n_k(i)$ is the corresponding additive noise.

The DC channel gain usually consists of both line-of-sight (LOS) and non-line-of-sight (NLOS) components. Due to the fact that the LOS component generally has a much larger electrical power than that of the NLOS component in most channel conditions, it is reasonable to only consider the LOS component when modeling the propagation of light over the spatial channel [30]. Therefore, assuming the LED follows a Lambertian radiation pattern, the DC channel gain between the LED and the k -th user can be calculated by [31]

$$h_k(0) = \frac{(m + 1)\rho A}{2\pi d_k^2} \cos^m(\psi_k) T(\phi_k) g(\phi_k) \cos(\phi_k), \tag{2}$$

where $m = -\ln 2 / \ln(\cos(\Psi))$ denotes the order of Lambertian emission, with Ψ being the semi-angle at half power of the LED; ρ is the PD responsivity, and A is the active area of the PD; d_k is the distance between the LED and the PD of the k -th user; ψ_k is the emission angle, and ϕ_k is the incident angle; $T(\phi_k)$ is the gain of the optical filter; $g(\phi_k) = \frac{r^2}{\sin^2 \Phi}$ is the gain of the optical lens, with r and Φ being the refractive index and the half-angle field-of-view (FOV) of the optical lens, respectively. Note that, if the incident light is outside the FOV of the receiver, $h_k(0)$ becomes zero.

Moreover, the amplitude attenuation coefficient $h_k(i)$ at the i -th subcarrier of the k -th user is determined not only by the low-pass frequency response of the LED, but also the set of subcarriers allocated to the k -th user. Hence, subcarrier allocation plays an important role in OFDM-based band-limited multi-user VLC systems [22].

In addition, the additive noise usually consists of both shot and thermal noises, and it is generally reasonable to model the additive noise as a real-valued zero-mean additive white Gaussian noise (AWGN) with power $\sigma^2 = N_0 B$, where N_0 is the power spectral density (PSD) of the AWGN and B is the signal bandwidth [32].

2.2. Principle of Rate-Splitting-Based GMA

In this subsection, we introduce the principle of the proposed rate-splitting-based GMA scheme for multi-user VLC systems. For a VLC system with more than two users, a hybrid OFDMA/GMA scheme can be considered to support the users by dividing them into pairs, where GMA is applied for the two users within each pair, while OFDMA is employed among different user pairs. Hence, a two-user VLC system is considered in the following.

Figure 1 illustrates a two-user VLC system applying conventional OMA and NOMA schemes, where the channel gains of the near user and the far user are denoted by h_n and h_f , respectively, with $h_n \geq h_f$. When OMA is applied in the two-user VLC system, the overall bandwidth B is divided and shared by the near and far users through subcarrier allocation during OFDM modulation. Due to the bandwidth partitioning, there is no IUI between the near and far users, but the available bandwidth of each user is inevitably reduced. In contrast, when NOMA is applied in the two-user VLC system, both the near user and the far user can utilize the overall bandwidth B , under the condition of severe IUI. Compared with the conventional OMA and NOMA schemes, our proposed rate-splitting-based GMA scheme can be seen as a generalized version of both OMA and NOMA, which achieves better bandwidth utilization than OMA and suffers less severe IUI than NOMA.

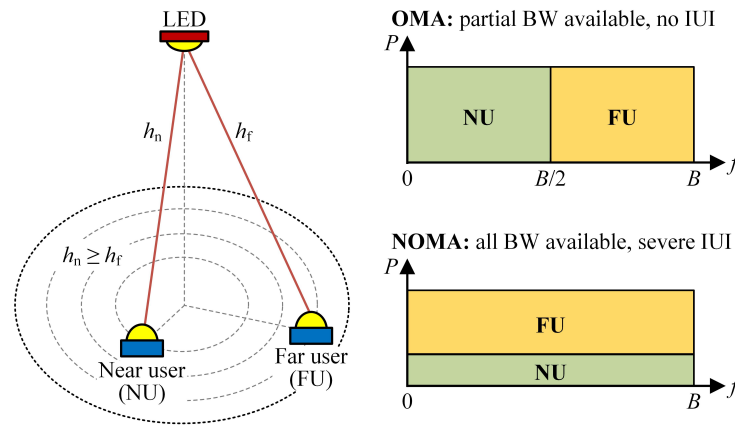


Figure 1. A two-user VLC system applying conventional OMA and NOMA.

Figure 2 shows the schematic diagram of a two-user VLC system applying the proposed rate-splitting-based GMA scheme. As we can see, the binary input data of each user are first split into two parts via a data splitter. More specifically, the binary input data of the near user b_n are split into $b_{n,1}$ and $b_{n,2}$, while the binary input data of the far user b_f are split into $b_{f,1}$ and $b_{f,2}$. After that, $b_{n,1}$, $b_{n,2}$, $b_{f,1}$ and $b_{f,2}$ are mapped into the quadrature amplitude modulation (QAM) constellation symbols $x_{n,1}$, $x_{n,2}$, $x_{f,1}$, and $x_{f,2}$, respectively. Here, $x_{n,1}$ and $x_{f,1}$ are separately transmitted in the OMA manner, while $x_{n,2}$ and $x_{f,2}$ are transmitted in the NOMA manner. Hence, $x_{n,2}$ and $x_{f,2}$ are combined together via power-domain SPC after power allocation. Letting P_n and P_f , respectively, denote the electrical powers allocated to transmit $x_{n,2}$ and $x_{f,2}$, the superposed electrical signal after SPC can be given by

$$x_2 = \sqrt{P_n}x_{n,2} + \sqrt{P_f}x_{f,2}, \tag{3}$$

where we have $P_{elec} = P_n + P_f$ and P_{elec} is the total allocated electrical power. Moreover, we further define $\alpha = P_n/P_f$ as the power allocation ratio (PAR) between the electrical powers allocated to, respectively, transmit $x_{n,2}$ and $x_{f,2}$, and hence, we have [22]

$$\begin{cases} P_f = \frac{P_{elec}}{1 + \alpha} \\ P_n = \frac{\alpha P_{elec}}{1 + \alpha} \end{cases} \tag{4}$$

Since the near user usually has a better channel condition than that of the far user, i.e., $h_n \geq h_f$, it is generally assumed that $P_n \leq P_f$, and therefore, we have $0 \leq \alpha \leq 1$ [14]. Subsequently, subcarrier allocation is performed for the transmission of the OMA parts $x_{n,1}$ and $x_{f,1}$ and the NOMA part x_2 . Considering the low-pass frequency response of practical VLC systems, the performance of the two-user VLC system using rate-splitting-based GMA largely depends on the adopted subcarrier allocation approach. After executing the inverse fast Fourier transform (IFFT) with the Hermitian symmetry (HS) constraint, parallel-to-serial (P/S) conversion, digital-to-analog (D/A) conversion, and DC bias addition, the resultant signal is directly used to modulate the LED for optical signal generation.

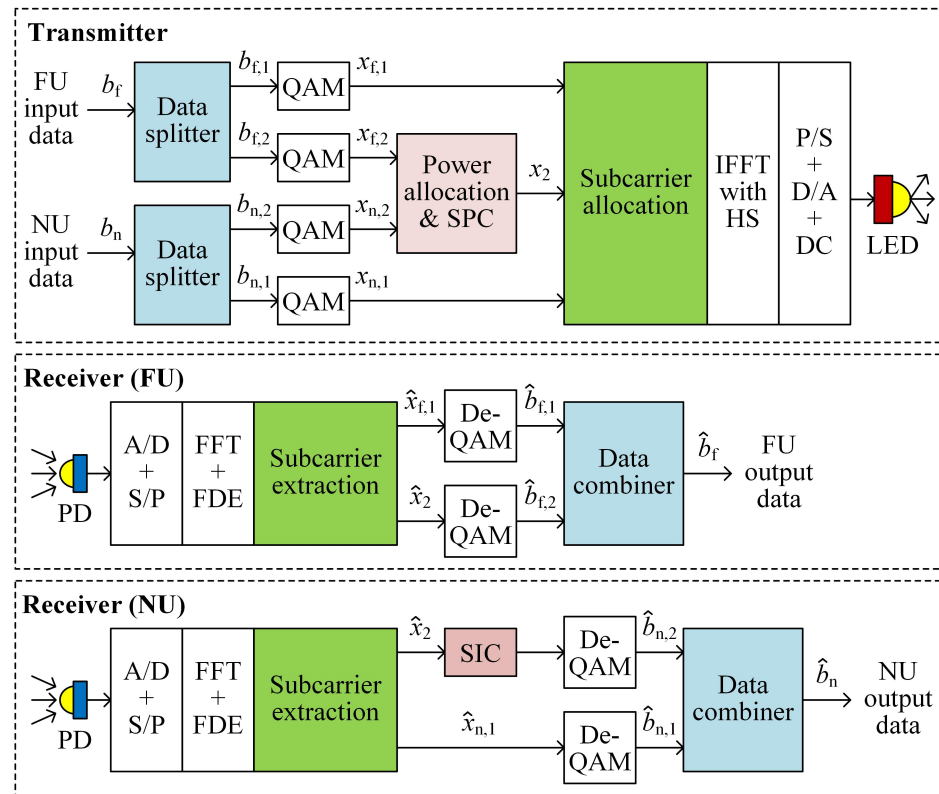


Figure 2. Schematic diagram of a two-user VLC system applying the proposed rate-splitting-based GMA scheme. FU: far user, NU: near user.

At the receiver side, each user uses a photo-detector (PD) to receive the optical signal, and the output signal is digitized via analog-to-digital (A/D) conversion. After serial-to-parallel (S/P) conversion, the forward FFT, and frequency-domain equalization (FDE), subcarrier extraction is carried out to extract the desired signals from the allocated subcarriers at each user. For the far user, the estimate of $x_{f,1}$, i.e., $\hat{x}_{f,1}$, is demapped to recover the binary data $\hat{b}_{f,1}$, while the estimate of x_2 , i.e., \hat{x}_2 , is also directly demapped to recover the binary data $\hat{b}_{f,2}$. The final output data of the far user \hat{b}_f is obtained by combining $\hat{b}_{f,1}$ and $\hat{b}_{f,2}$ together via a data combiner. For the near user, the estimate of $x_{n,1}$, i.e., $\hat{x}_{n,1}$, is demapped to recover the binary data $\hat{b}_{n,1}$, while the estimate of x_2 , i.e., \hat{x}_2 , is first utilized to conduct SIC, and the resultant signal is then demapped to recover the binary data $\hat{b}_{n,2}$. By combining $\hat{b}_{n,1}$ and $\hat{b}_{n,2}$ together through a data combiner, the final output data of the near user \hat{b}_n can be achieved. It should be noted that the SIC at the near user might not always be perfect, and error propagation due to imperfect SIC might occur [16].

Figure 3 illustrates the transmitted OFDM spectrum employing different multiple access schemes in the band-limited two-user VLC system. When OMA is applied, as shown in Figure 3a, it is generally assumed that the low-frequency band (LFB) is allocated to the near user, while the high-frequency band (HFB) is allocated to the far user, in order to maximize the overall achievable rate of the system [10]. In contrast, when NOMA is adopted, as shown in Figure 3b, both the near user and the far user can utilize the overall bandwidth, and hence, subcarrier allocation is not required. To efficiently implement the proposed rate-splitting-based GMA scheme in the band-limited two-user VLC system, the overall bandwidth needs to be divided into three bands, i.e., LFB, medium-frequency band (MFB), and HFB, and subcarrier allocation among two OMA parts and one NOMA part should be considered according to the low-pass frequency response of the system. Under the general assumption that the OMA band allocated to the near user should have a lower frequency than that allocated to the far user, the potential transmitted OFDM spectrum using rate-splitting-based GMA mainly has three forms with respect to the three locations of the NOMA part. More specifically, the first one is illustrated in Figure 3c, where the

NOMA part is located in the LFB, the second one is illustrated in Figure 3d, where the NOMA part is located in the MFB, and the third one is illustrated in Figure 3e, where the NOMA part is located in the HFB.

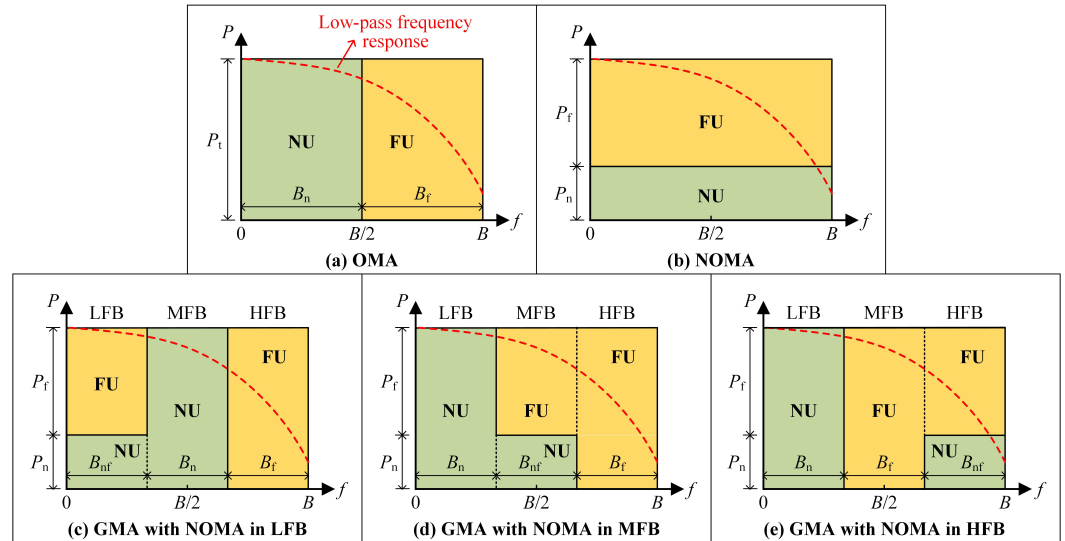


Figure 3. Illustration of transmitted OFDM spectrum employing: (a) OMA, (b) NOMA, (c) GMA with NOMA in LFB, (d) GMA with NOMA in MFB, and (e) GMA with NOMA in HFB. LFB: low-frequency band, MFB: medium-frequency band, HFB: high-frequency band.

Letting B_n , B_f , and B_{nf} , respectively, denote the bandwidths of the near user’s OMA band, the far user’s OMA band, and the NOMA band, we have $B_n + B_f + B_{nf} = B$. Moreover, we further define the bandwidth allocation ratio (BAR) of the near user’s OMA band as $\beta_n = 2B_n/B$ and the BAR of the far user’s OMA band as $\beta_f = 2B_f/B$, with $0 \leq \beta_n \leq 1$ and $0 \leq \beta_f \leq 1$. Specifically, the proposed rate-splitting-based GMA scheme becomes OMA with equal bandwidth allocation if $\beta_n = \beta_f = 1$, while the proposed rate-splitting-based GMA scheme becomes NOMA if $\beta_n = \beta_f = 0$. It can be observed from Figure 3 that the performance of the proposed rate-splitting-based GMA scheme depends on the BARs β_n and β_f , the PAR α for the NOMA band, and the locations of the NOMA band. Therefore, the overall achievable rate of the band-limited two-user VLC system applying rate-splitting-based GMA can be maximized by optimizing β_n , β_f , α and the locations of the NOMA band.

2.3. Achievable Rate

The overall achievable rate of the band-limited two-user VLC system applying rate-splitting-based GMA can be obtained by the summation of the achievable rates of both the near user and the far user. For each user, the achievable rate also consists of both the OMA part and the NOMA part. As shown in Figure 3c–e, the overall bandwidth of the OFDM signal is divided into three bands, i.e., LFB, MFB, and HFB. Hence, the data subcarriers of the OFDM signal are also divided into three subsets accordingly.

Let $\mathcal{S} = \{s_n^1, s_n^2, \dots, s_n^K\}$ represent the overall available subcarrier set for data transmission, with K denoting the total number of data subcarriers. For an overall signal bandwidth B , the occupied bandwidth of each subcarrier is given by $B_{sc} = B/K$. Let $\mathcal{S}_n = \{s_n^1, s_n^2, \dots, s_n^{K_n}\}$, $\mathcal{S}_f = \{s_f^1, s_f^2, \dots, s_f^{K_f}\}$, and $\mathcal{S}_{nf} = \{s_{nf}^1, s_{nf}^2, \dots, s_{nf}^{K_{nf}}\}$, respectively, denote the subcarrier sets allocated to the near user’s OMA part, the far user’s OMA part, and the NOMA part, where K_n , K_f , and K_{nf} represent the numbers of subcarriers in the corresponding subcarrier sets, and hence, we have $\mathcal{S}_n \cap \mathcal{S}_f \cap \mathcal{S}_{nf} = \emptyset$, $\mathcal{S}_n \cup \mathcal{S}_f \cup \mathcal{S}_{nf} = \mathcal{S}$, and $K_n + K_f + K_{nf} = K$. Moreover, the BARs β_n and β_f can also be re-defined as $\beta_n = 2K_n/K$ and $\beta_f = 2K_f/K$.

At the receiver side of the far user, as can be seen from Figure 2, the OMA part $\hat{x}_{f,1}$ and the NOMA part \hat{x}_2 are both directly demapped. Hence, the received signal-to-noise ratio (SNR) of the far user at the i -th subcarrier can be obtained by

$$\gamma_f^i = \begin{cases} \frac{(h_f(0)h_f(i))^2 P_{elec}}{\sigma^2}, & i \in \mathcal{S}_f \\ \frac{(h_f(0)h_f(i))^2 P_f}{(h_f(0)h_f(i))^2 P_n + \sigma^2}, & i \in \mathcal{S}_{nf} \end{cases}, \quad (5)$$

where $h_f(0)$ and $h_f(i)$ denote the DC channel gain and the amplitude attenuation coefficient at the i -th subcarrier of the far user, respectively. By substituting (4) in (5), we have

$$\gamma_f^i = \begin{cases} (h_f(0)h_f(i))^2 \gamma_{tx}, & i \in \mathcal{S}_f \\ \frac{(h_f(0)h_f(i))^2 \gamma_{tx}}{\alpha (h_f(0)h_f(i))^2 \gamma_{tx} + 1 + \alpha}, & i \in \mathcal{S}_{nf} \end{cases}, \quad (6)$$

where $\gamma_{tx} = P_{elec} / \sigma^2$ denotes the transmitted SNR [33].

Moreover, at the receiver side of the near user, as shown in Figure 2, the OMA part $\hat{x}_{n,1}$ is directly demapped, while SIC is first performed for the the NOMA part \hat{x}_2 before demapping. As a result, considering the error propagation effect caused by imperfect SIC, the received SNR of the near user at the i -th subcarrier can be achieved by

$$\gamma_n^i = \begin{cases} \frac{(h_n(0)h_n(i))^2 P_{elec}}{\sigma^2}, & i \in \mathcal{S}_n \\ \frac{(h_n(0)h_n(i))^2 P_n}{\zeta (h_n(0)h_n(i))^2 P_f + \sigma^2}, & i \in \mathcal{S}_{nf} \end{cases}, \quad (7)$$

where $h_n(0)$ and $h_n(i)$ represent the DC channel gain and the amplitude attenuation coefficient at the i -th subcarrier of the near user, respectively, and ζ denotes the error propagation ratio (EPR). Similarly, by substituting (4) in (7), we have

$$\gamma_n^i = \begin{cases} (h_n(0)h_n(i))^2 \gamma_{tx}, & i \in \mathcal{S}_n \\ \frac{\alpha (h_n(0)h_n(i))^2 \gamma_{tx}}{\zeta (h_n(0)h_n(i))^2 \gamma_{tx} + 1 + \alpha}, & i \in \mathcal{S}_{nf} \end{cases}. \quad (8)$$

Based on (6) and (8), the achievable rates of the near user and the far user can be, respectively, calculated as follows:

$$R_n = \frac{B}{K} \sum_{i \in [\mathcal{S}_n, \mathcal{S}_{nf}]} \log_2(1 + \gamma_n^i), \quad (9)$$

$$R_f = \frac{B}{K} \sum_{i \in [\mathcal{S}_f, \mathcal{S}_{nf}]} \log_2(1 + \gamma_f^i), \quad (10)$$

and hence, the achievable sum rate of the near and far users can be given by

$$R = R_n + R_f = \frac{B}{K} \left(\sum_{i \in [\mathcal{S}_n, \mathcal{S}_{nf}]} \log_2(1 + \gamma_n^i) + \sum_{i \in [\mathcal{S}_f, \mathcal{S}_{nf}]} \log_2(1 + \gamma_f^i) \right). \quad (11)$$

3. Results and Discussion

In this section, theoretical and simulation investigations were first performed to find the optimal rate-splitting-based GMA scheme among the three candidates, as shown in Figure 3c–e. Then, theoretical, simulation, and experimental results are presented to

evaluate and compare the achievable rate of a practical band-limited VLC system applying the optimal rate-splitting-based GMA scheme and other benchmark schemes.

3.1. Optimization of Rate-Splitting-Based GMA Schemes

To obtain the optimal rate-splitting-based GMA scheme, we considered a practical band-limited two-user VLC system adopting the three candidate rate-splitting-based GMA schemes, as shown in Figure 3c–e. In this work, our goal was to find the optimal rate-splitting-based GMA scheme by identifying the optimal β_n and β_f values with optimal power allocation for the NOMA part, and the optimization was performed via exhaustive search using computer simulations. The formulation of the optimization problem and the derivation of the optimal solution are outside the scope of this work, which will be investigated in our future work.

Figure 4a depicts the geometric configuration of the two-user VLC system, where the near user is right under the LED with a vertical separation of 2.15 m, while the horizontal separation between the near user and the far user is denoted by δ . The key simulation parameters of the band-limited two-user VLC system are listed in Table 3, and the simulations were performed by using MATLAB. The semi-angle at half power of the LED and the half-angle FOV of the optical lens were both 70° ; the gain of the optical filter was 0.9; the refractive index of the optical lens was 1.5; the responsivity and the active area of the PD were 0.53 A/W and 1 cm², respectively. Moreover, the signal bandwidth was 39.1 MHz, and the noise PSD was 10^{-22} A²/Hz. To reflect the low-pass nature of practical VLC systems, we adopted a practically measured low-pass frequency response in the simulations, which is illustrated in Figure 4b, and the corresponding -3 dB bandwidth of the VLC system was 14.8 MHz.

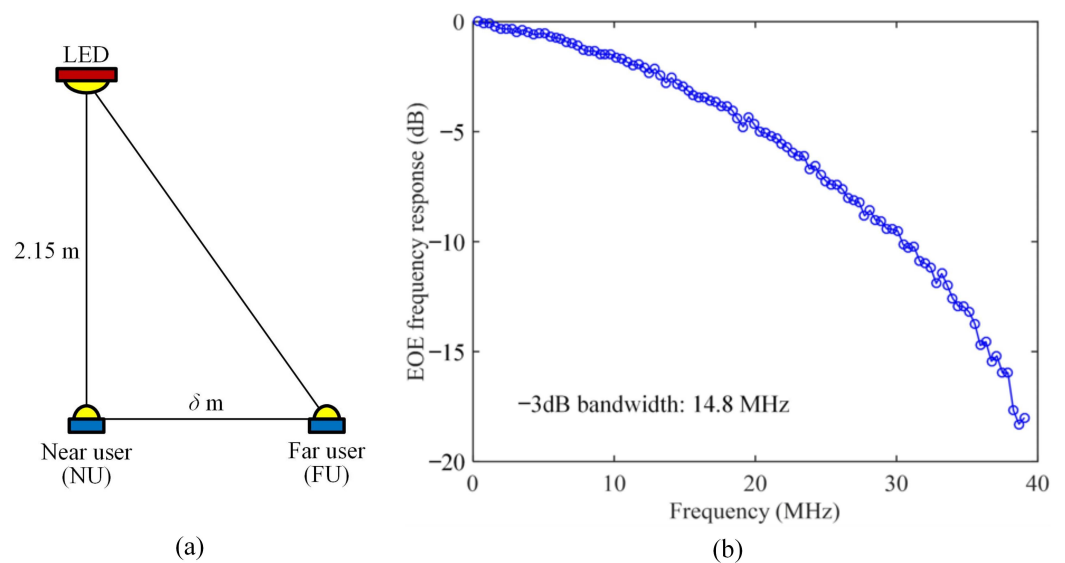


Figure 4. Simulation setup of a two-user VLC system: (a) geometric configuration and (b) system frequency response.

Table 3. Simulation parameters.

Parameter	Value
Vertical separation	2.15 m
Semi-angle at half power of LED	70°
Gain of optical filter	0.9
Refractive index of optical lens	1.5
Half-angle FOV of optical lens	70°
Responsivity of PD	0.53 A/W
Active area of PD	1 cm ²
Signal bandwidth	39.1 MHz
Noise power spectral density	10 ⁻²² A ² /Hz

Figure 5 shows the contour plot of the achievable sum rate versus BARs β_n and β_f for three candidate rate-splitting-based GMA schemes with different error propagation levels, where the transmitted SNR was $\gamma_{tx} = 118$ dB and the user separation was $\delta = 1.5$ m. For the first candidate rate-splitting-based GMA scheme, i.e., GMA with NOMA in LFB, as shown in Figure 5a–c, the maximum achievable sum rate was achieved with $\beta_n = 1$ and $\beta_f = 0$ for both $\zeta = 0$ and 0.05, while the maximum achievable sum rate was obtained with $\beta_n = 1$ and $\beta_f = 0.2$ for $\zeta = 0.1$. In contrast, for the second/third candidate rate-splitting-based GMA schemes, i.e., GMA with NOMA in MFB/HFB, as can be seen from Figure 5d–i, the maximum achievable sum rate was always achieved with $\beta_n = 1$ and $\beta_f = 0$ for three error propagation levels, i.e., $\zeta = 0, 0.05,$ and 0.1. Hence, for the cases that GMA with NOMA in MFB and HFB, the optimal β_f values were both 0, which indicates that the far user’s data were only transmitted in the NOMA manner and the resultant GMA scheme only consisted of two bands, i.e., an LFB transmitting the near user’s data in the OMA manner and an HFB transmitting both the near user’s data and the far user’s data in the NOMA manner. Since GMA with NOMA in MFB and GMA with NOMA in HFB became exactly the same when $\beta_f = 0$, we only needed to compare GMA with NOMA in LFB and GMA with NOMA in HFB so as to identify the optimal rate-splitting-based GMA scheme.

According to the obtained optimal combination BARs β_n and β_f for each case, Figure 6 shows the achievable sum rate versus the transmitted SNR for different GMA schemes with different error propagation levels and user separations. For $\zeta = 0$, as shown in Figure 6a, nearly the same achievable sum rate can be achieved by GMA with NOMA in LFB and GMA with NOMA in HFB for two user separations, i.e., $\delta = 0.5$ and 1.5 m. However, for $\zeta = 0.05$ and 0.1, as can be seen from Figure 6b,c, GMA with NOMA in HFB achieved a higher sum rate than GMA with NOMA in LFB, especially when ζ and δ were relatively large. Therefore, it can be clearly observed from Figure 6 that GMA with NOMA in HFB is the optimal scheme, which can always achieve the highest sum rate among all the candidate rate-splitting-based GMA schemes. Figure 7 depicts the obtained optimal rate-splitting-based GMA scheme with NOMA in HFB, $\beta_n = 1$ and $\beta_f = 0$, and hence, we can have $B_n = B_{nf} = B/2$ and $B_f = 0$. Moreover, it can also be found from Figure 6a–c that the simulation results agreed well with the theoretical results.

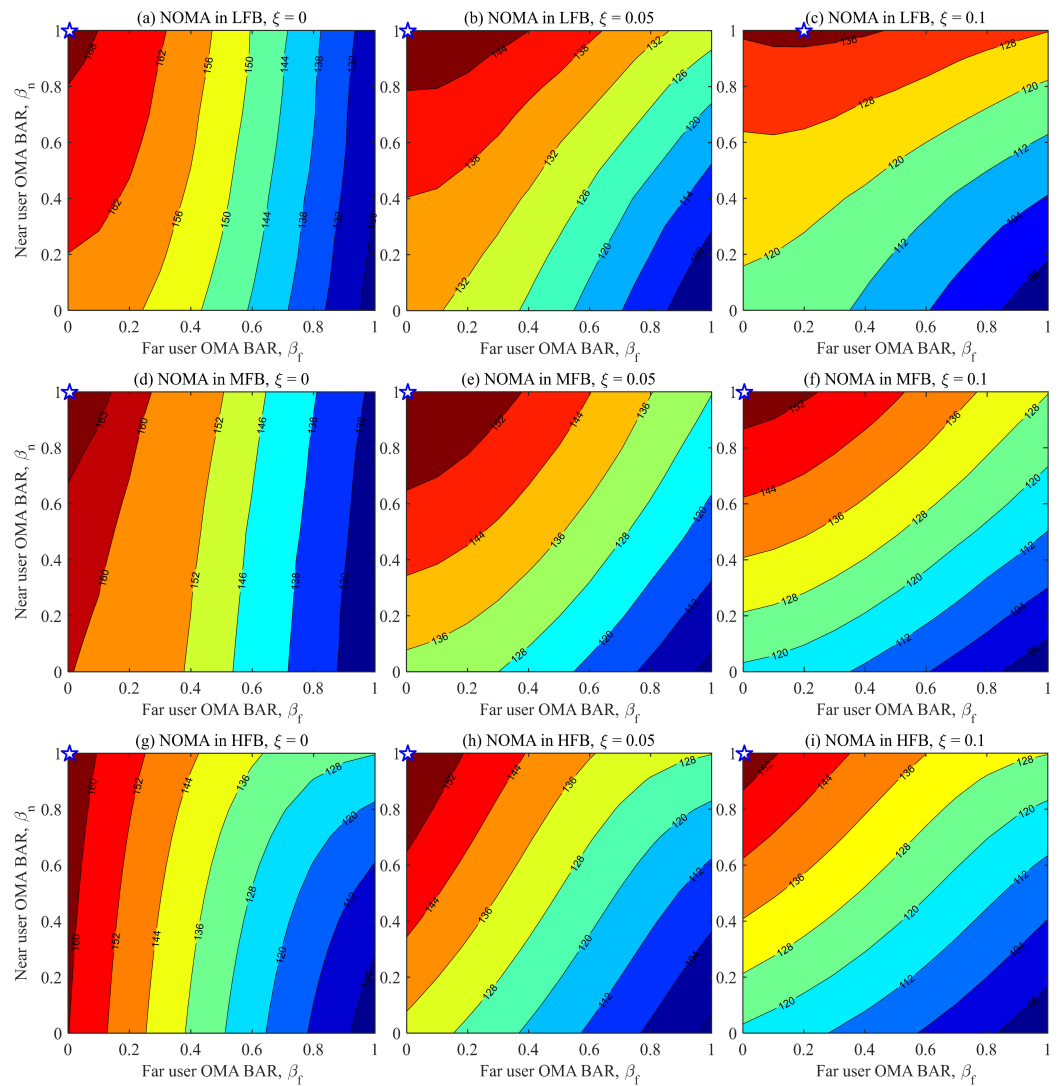


Figure 5. Contour plot of the achievable sum rate (Mbit/s) for (a) NOMA in LFB, $\zeta = 0$, (b) NOMA in LFB, $\zeta = 0.05$, (c) NOMA in LFB, $\zeta = 0.1$, (d) NOMA in MFB, $\zeta = 0$, (e) NOMA in MFB, $\zeta = 0.05$, (f) NOMA in MFB, $\zeta = 0.1$, (g) NOMA in HFB, $\zeta = 0$, (h) NOMA in HFB, $\zeta = 0.05$, and (i) NOMA in HFB, $\zeta = 0.1$, where the optimal combination of β_n and β_f to achieve the maximum sum rate for each case is highlighted by the blue star.

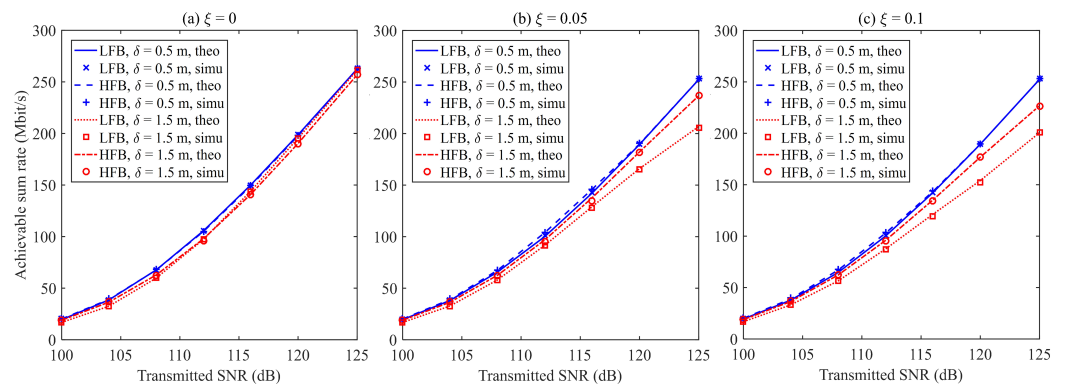


Figure 6. Achievable sum rate vs. transmitted SNR for different GMA schemes and different user separations with (a) $\zeta = 0$, (b) $\zeta = 0.05$, and (c) $\zeta = 0.1$.

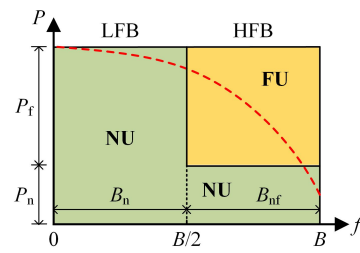


Figure 7. Optimal GMA scheme over band-limited low-pass VLC channel.

3.2. Performance Evaluation and Comparison

Next, we further evaluated and compared the performance of a practical band-limited two-user VLC system applying the obtained optimal rate-splitting-based GMA scheme and two state-of-the-art benchmark schemes including OMA and NOMA via theoretical analysis, simulations, and experiments. The simulation setup is shown in Figure 4a, and the simulation tool was MATLAB; the detailed simulation parameters can be found in Table 3. Moreover, the experimental setup of a two-user VLC system is depicted in Figure 8a, and the photo of the experimental testbed is given in Figure 8b.

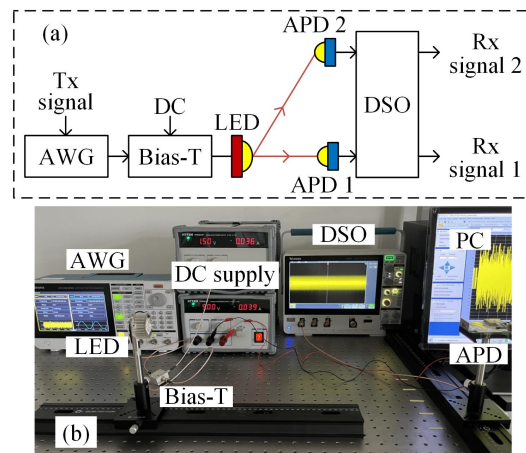


Figure 8. (a) Experimental setup of a two-user VLC system and (b) the photo of the experimental testbed.

In our experiments, the transmitted signal was first generated offline by MATLAB and then sent to an arbitrary waveform generator (AWG, Tektronix AFG31102) with a sampling rate of 100 MSa/s. Subsequently, the AWG output signal was added with a 36 mA DC bias current via a bias-tee (bias-T, MiniCircuits, ZFBT-6GW+), and the resultant signal was utilized to drive a commercially available LED. At the receiver side, two users were located within the coverage of the VLC system, where each user was equipped with an avalanche photo-diode (APD, Hamamatsu C12702-12) to detect the optical signal. The transmission distance between the LED and the two APDs was 60 cm. It can be seen that APD 1 directly faced the LED, while the separation between APD 1 and APD 2 is also denoted by δ , which ranged from 5 to 20 cm. The detected electrical signals from two APDs were recorded by a two-channel digital storage oscilloscope (DSO, LeCroy WaveSurfer 432) with a sampling rate of 500 MSa/s, which were further processed offline via MATLAB. In the digital OFDM modulation at the transmitter side, the size of the IFFT was set to 256, and a total of 100 (i.e., 2nd to the 101st) subcarriers were adopted for data transmission. Hence, the bandwidth of the generated OFDM signal from the AWG was 39.1 MHz. The measured frequency response of the experimental system is shown in Figure 4b with a -3 dB bandwidth of 14.8 MHz.

Figure 9a–c show the theoretical and simulation sum rate versus the transmitted SNR for $\zeta = 0, 0.05, \text{ and } 0.1$, respectively, where $\delta = 1.5$ m and $B = 39.1$ MHz. For $\zeta = 0$, which

indicates perfect SIC without error propagation, it can be found that GMA outperformed NOMA in terms of the achievable sum rate when the transmitted SNR was relatively small, while nearly the same sum rate can be achieved by GMA and NOMA when the transmitted SNR reached 120 dB. Moreover, GMA always achieved a higher sum rate than OMA, and the sum rate gain became more significant when the transmitted SNR was gradually increased. For $\zeta = 0.05$, the achievable sum rate of NOMA was substantially reduced, which became comparable to OMA. For $\zeta = 0.1$, which means the error propagation is severe, NOMA even performed worse than OMA, especially when the transmitted SNR was relatively large. Figure 9d–f show the experimental sum rate versus the peak-to-peak voltage (V_{pp}) of the AWG output signal for $\zeta = 0, 0.05$, and 0.1 , respectively, where $\delta = 20$ cm and $B = 39.1$ MHz. Similarly, as we can see, NOMA achieved a comparable sum rate as GMA for $\zeta = 0$ with a large V_{pp} , while the achievable sum rate of NOMA was greatly reduced when the error propagation became severe. It can be clearly observed from Figure 9a–f that the optimal rate-splitting-based GMA scheme always achieved the highest sum rate, and its performance gain over NOMA was much more significant when the error propagation was more severe.

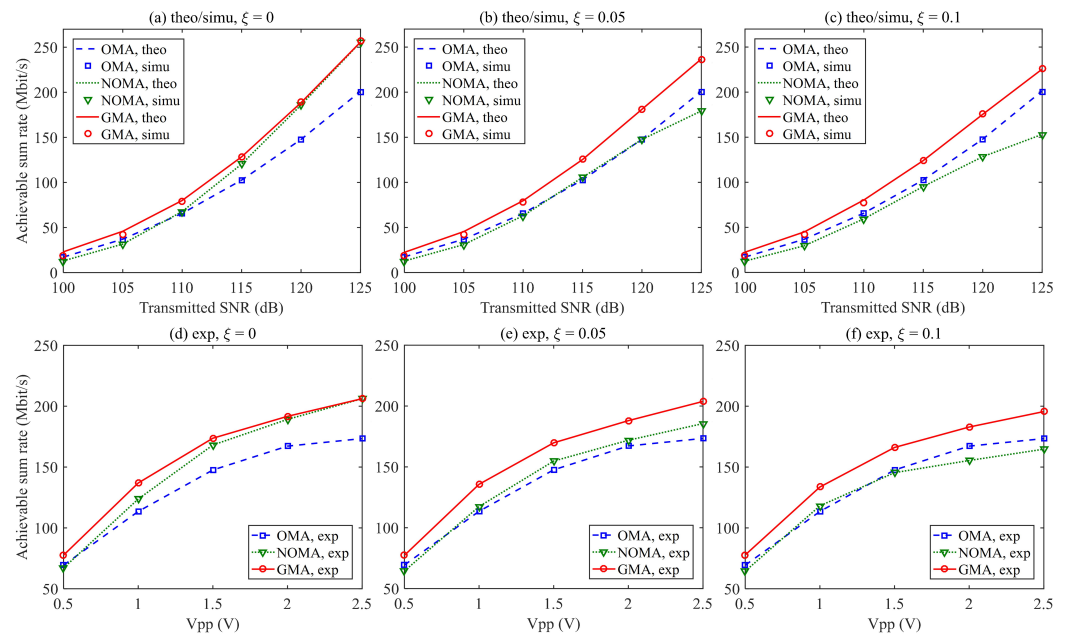


Figure 9. Theoretical and simulation sum rate vs. transmitted SNR for (a) $\zeta = 0$, (b) $\zeta = 0.05$, (c) $\zeta = 0.1$, and experimental sum rate vs. V_{pp} for (d) $\zeta = 0$, (e) $\zeta = 0.05$, and (f) $\zeta = 0.1$.

Figure 10a–c show the theoretical and simulation sum rate versus the user separation for $\zeta = 0, 0.05$, and 0.1 , respectively, where $\gamma_{tx} = 118$ dB and $B = 39.1$ MHz. For $\zeta = 0$, NOMA and GMA achieved nearly the same sum rate when the user separation was less than 1 m, and GMA gradually outperformed NOMA when the user separation was larger than 1 m. Moreover, the achievable sum rate of OMA was reduced rapidly with the increase of the user separation. For large ζ values of 0.05 and 0.1 , the achievable rate of NOMA was substantially reduced. Figure 10d–f show the experimental sum rate versus the user separation for $\zeta = 0, 0.05$ and 0.1 , respectively, where $V_{pp} = 1.5$ V and $B = 39.1$ MHz. It can be seen that the obtained experimental results demonstrated the same trend as that shown by the theoretical and simulation results. Hence, in comparison to OMA and NOMA, the optimal rate-splitting-based GMA scheme was able to achieve a substantially improved sum rate when the two users had a large separation.

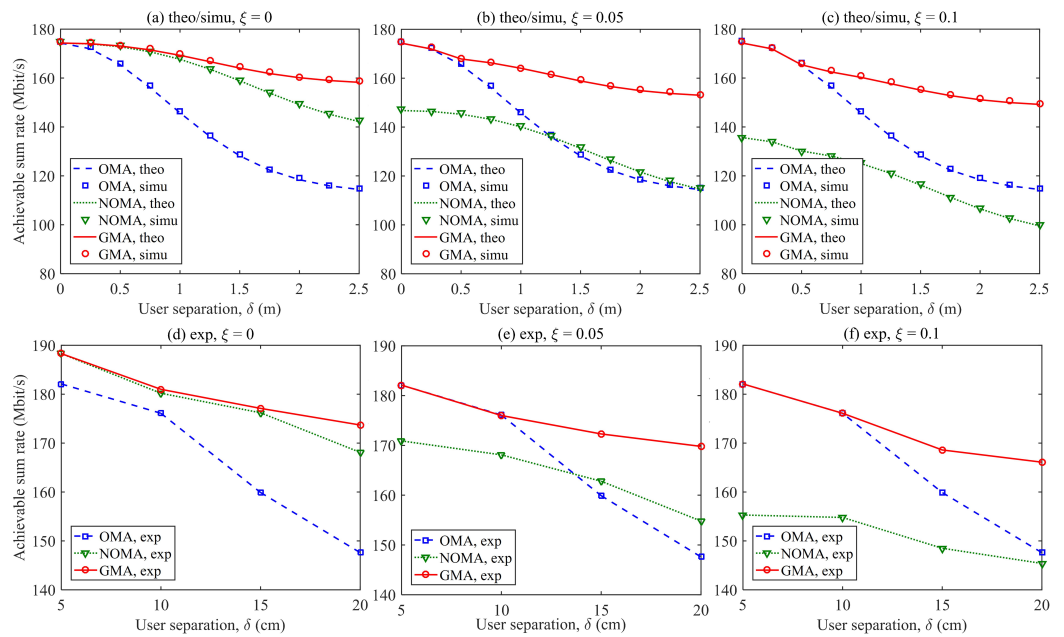


Figure 10. Theoretical and simulation sum rate vs. user separation for (a) $\xi = 0$, (b) $\xi = 0.05$, (c) $\xi = 0.1$, and experimental sum rate vs. user separation for (d) $\xi = 0$, (e) $\xi = 0.05$, and (f) $\xi = 0.1$.

Figure 11a shows the theoretical and simulation sum rate versus the EPR ξ , where $\gamma_{tx} = 118$ dB, $\delta = 1.5$ m, and $B = 39.1$ MHz. As we can see, the achievable sum rate of GMA was only slightly reduced from 164.6 to 150.1 Mbit/s when ξ was increased from 0 to 0.2, and the corresponding sum rate reduction ratio was as low as 8.8%. In contrast, the achievable sum rate of NOMA was significantly reduced from 159.5 to 98.9 Mbit/s, which indicated a sum rate reduction ratio of as high as 38.0%. Figure 11b shows the experimental sum rate versus the EPR ξ , where $V_{pp} = 1.5$ V, $\delta = 20$ cm, and $B = 39.1$ MHz. Similarly, when ξ was increased from 0 to 0.2, the obtained sum rate reduction ratios of GMA and NOMA were 7.5% and 31.4%, respectively. Therefore, compared with NOMA, the optimal rate-splitting-based GMA scheme exhibited greatly enhanced robustness against imperfect SIC-induced error propagation.

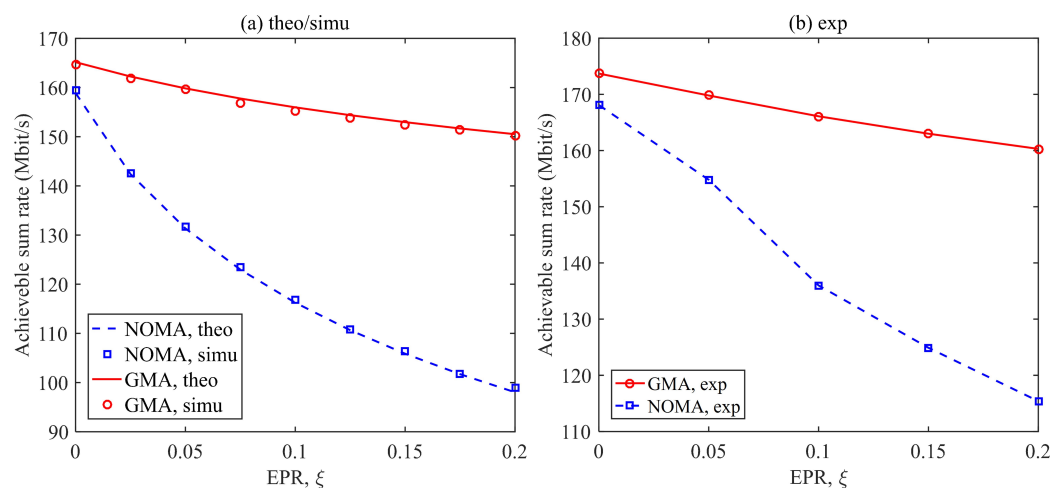


Figure 11. Achievable sum rate vs. EPR for NOMA and GMA: (a) theoretical and simulation results and (b) experimental results.

Moreover, it can be seen from Figures 9–11 that the simulation results slightly underestimated the experimental ones, which was mainly because that the experimentally received SNRs were slightly lower than the corresponding received SNRs in the simulation

system. Despite this difference, our primary objective of this study was to investigate the general tendency in the performance of our proposed system under various conditions. Although the simulation and experimental results may differ quantitatively, we believe that the qualitative trends observed in both cases are reliable and useful for evaluating the feasibility and superiority of our proposed scheme.

4. Conclusions

In this paper, we proposed and evaluated a novel rate-splitting-based GMA scheme for band-limited multi-user VLC systems. As a generalized version of both OMA and NOMA, GMA achieved better bandwidth utilization than OMA and suffered less severe interference than NOMA. By optimizing the BARs of the two OMA bands through theoretical analysis and computer simulations, we successfully obtained the optimal rate-splitting-based GMA scheme among all the three candidate schemes. Moreover, our theoretical, simulation, and experimental results further demonstrated that the optimal rate-splitting-based GMA scheme can always achieve the highest sum rate under various channel conditions, user separations, and error propagation levels. More specifically, the optimal rate-splitting-based GMA scheme greatly outperformed NOMA when the user separation was relatively large, which also exhibited excellent robustness against error propagation caused by imperfect SIC. Therefore, the optimal rate-splitting-based GMA scheme can be a promising candidate for practical band-limited multi-user VLC systems. In our future work, we will investigate a hybrid OFDMA/GMA scheme to support more than two users in a practical VLC system, and efficient user pairing approaches will be further proposed.

Author Contributions: Formal analysis, Y.T., C.C. and M.L.; funding acquisition, C.C.; investigation, Y.T. and P.D.; methodology, H.Y.F.; project administration, C.C.; resources, H.Y.F.; software, P.D.; supervision, C.C., M.L. and H.Y.F.; validation, Y.T.; writing—original draft, Y.T.; writing—review and editing, C.C., M.L., P.D. and H.Y.F. All authors have read and agreed to the published version of the manuscript.

Funding: This research was funded by the National Natural Science Foundation of China (62271091), the Natural Science Foundation of Chongqing (cstc2021jcyj-msxmX0480), and the Sichuan Provincial S&T Projects (2020YFH0054).

Institutional Review Board Statement: Not applicable.

Informed Consent Statement: Not applicable.

Data Availability Statement: Not applicable.

Acknowledgments: The authors would like to thank the anonymous Reviewers for their valuable comments and suggestions.

Conflicts of Interest: The authors declare no conflict of interest.

References

1. Yang, P.; Xiao, Y.; Xiao, M.; Li, S. 6G wireless communications: Vision and potential techniques. *IEEE Netw.* **2019**, *33*, 70–75. [[CrossRef](#)]
2. Cogalan, T.; Haas, H. Why would 5G need optical wireless communications? In Proceedings of the IEEE 28th Annual International Symposium on Personal, Indoor, and Mobile Radio Communications (PIMRC), Montreal, QC, Canada, 8–13 October 2017; pp. 1–6.
3. Komine, T.; Nakagawa, M. Fundamental analysis for visible-light communication system using LED lights. *IEEE Trans. Consum. Electron.* **2004**, *50*, 100–107. [[CrossRef](#)]
4. Chi, N.; Zhou, Y.; Wei, Y.; Hu, F. Visible light communication in 6G: Advances, challenges, and prospects. *IEEE Veh. Technol. Mag.* **2020**, *15*, 93–102. [[CrossRef](#)]
5. Demirkol, I.; Camps-Mur, D.; Paradells, J.; Combalia, M.; Popoola, W.; Haas, H. Powering the Internet of Things through light communication. *IEEE Commun. Mag.* **2019**, *57*, 107–113. [[CrossRef](#)]
6. Obeed, M.; Salhab, A.M.; Alouini, M.S.; Zummo, S.A. On optimizing VLC networks for downlink multi-user transmission: A survey. *IEEE Commun. Surv. Tutor.* **2019**, *21*, 2947–2976. [[CrossRef](#)]
7. Eltokhey, M.W.; Khalighi, M.A.; Ghassemlooy, Z. Optimization of receivers' field of views in multi-user VLC networks: A bio-inspired approach. *IEEE Wirel. Commun.* **2022**, *29*, 132–139. [[CrossRef](#)]

8. Linnartz, J.P.M.; Deng, X.; Alexeev, A.; Mardanikorani, S. Wireless communication over an LED channel. *IEEE Commun. Mag.* **2020**, *58*, 77–82. [[CrossRef](#)]
9. Abdelhady, A.M.; Amin, O.; Chaaban, A.; Shihada, B.; Alouini, M.S. Downlink resource allocation for dynamic TDMA-based VLC systems. *IEEE Trans. Wirel. Commun.* **2019**, *18*, 108–120. [[CrossRef](#)]
10. Sung, J.Y.; Yeh, C.H.; Chow, C.W.; Lin, W.F.; Liu, Y. Orthogonal frequency-division multiplexing access (OFDMA) based wireless visible light communication (VLC) system. *Opt. Commun.* **2015**, *355*, 261–268. [[CrossRef](#)]
11. Lian, J.; Brandt-Pearce, M. Multiuser visible light communication systems using OFDMA. *J. Lightw. Technol.* **2020**, *38*, 6015–6023. [[CrossRef](#)]
12. Qiu, Y.; Chen, S.; Chen, H.H.; Meng, W. Visible light communications based on CDMA technology. *IEEE Wirel. Commun.* **2018**, *25*, 178–185. [[CrossRef](#)]
13. Chen, D.; Fan, K.; Wang, J.; Lu, H.; Jin, J.; Feng, L.; Chen, H.; Xue, Z.; Wang, Y. Integrated visible light communication and positioning CDMA system employing modified ZCZ and Walsh code. *Opt. Express* **2022**, *30*, 40455–40469. [[CrossRef](#)]
14. Marshoud, H.; Kapinas, V.M.; Karagiannidis, G.K.; Muhaidat, S. Non-orthogonal multiple access for visible light communications. *IEEE Photonics Technol. Lett.* **2016**, *28*, 51–54. [[CrossRef](#)]
15. Marshoud, H.; Sofotasios, P.C.; Muhaidat, S.; Karagiannidis, G.K.; Sharif, B.S. On the performance of visible light communication systems with non-orthogonal multiple access. *IEEE Trans. Wirel. Commun.* **2017**, *16*, 6350–6364. [[CrossRef](#)]
16. Chen, C.; Zhong, W.D.; Yang, H.; Du, P.; Yang, Y. Flexible-rate SIC-free NOMA for downlink VLC based on constellation partitioning coding. *IEEE Wirel. Commun. Lett.* **2019**, *8*, 568–571. [[CrossRef](#)]
17. Wu, T.; Wang, Z.; Han, S.; Yu, J.; Jiang, Y. Demonstration of performance improvement in multi-user NOMA VLC system using joint transceiver optimization. *Photonics* **2022**, *9*, 168. [[CrossRef](#)]
18. Lin, B.; Lai, Q.; Ghassemlooy, Z.; Tang, X. A machine learning based signal demodulator in NOMA-VLC. *J. Light. Technol.* **2021**, *39*, 3081–3087. [[CrossRef](#)]
19. Chen, C.; Fu, S.; Jian, X.; Liu, M.; Deng, X.; Ding, Z. NOMA for energy-efficient LiFi-enabled bidirectional IoT communication. *IEEE Trans. Commun.* **2021**, *69*, 1693–1706. [[CrossRef](#)]
20. Yin, L.; Popoola, W.O.; Wu, X.; Haas, H. Performance evaluation of non-orthogonal multiple access in visible light communication. *IEEE Trans. Commun.* **2016**, *64*, 5162–5175. [[CrossRef](#)]
21. Lin, B.; Ye, W.; Tang, X.; Ghassemlooy, Z. Experimental demonstration of bidirectional NOMA-OFDMA visible light communications. *Opt. Express* **2017**, *25*, 4348–4355. [[CrossRef](#)]
22. Chen, C.; Tang, Y.; Cai, Y.; Liu, M. Fairness-aware hybrid NOMA/OFDMA for band-limited multi-user VLC systems. *Opt. Express* **2021**, *29*, 42265–42275. [[CrossRef](#)]
23. Chen, C.; Zhong, W.D.; Yang, H.; Du, P. On the performance of MIMO-NOMA-based visible light communication systems. *IEEE Photonics Technol. Lett.* **2018**, *30*, 307–310. [[CrossRef](#)]
24. Chen, C.; Zhang, R.; Wen, W.; Liu, M.; Du, P.; Yang, Y.; Ruan, X. Hybrid 3DMA for multi-user MIMO-VLC. *J. Opt. Commun. Netw.* **2022**, *14*, 780–791. [[CrossRef](#)]
25. Naser, S.; Sofotasios, P.C.; Bariah, L.; Jaafar, W.; Muhaidat, S.; Al-Qutayri, M.; Dobre, O.A. Rate-splitting multiple access: Unifying NOMA and SDMA in MISO VLC channels. *IEEE Open J. Veh. Technol.* **2020**, *1*, 393–413. [[CrossRef](#)]
26. Tao, S.; Yu, H.; Li, Q.; Tang, Y.; Zhang, D. One-layer rate-splitting multiple access with benefits over power-domain NOMA in indoor multi-cell visible light communication networks. In Proceedings of the IEEE International Conference on Communications Workshops (ICC Workshops), Dublin, Ireland, 7–11 June 2020; pp. 1–7.
27. Xing, F.; He, S.; Leung, V.C.; Yin, H. Energy efficiency optimization for rate-splitting multiple access-based indoor visible light communication networks. *IEEE J. Sel. Areas Commun.* **2022**, *40*, 1706–1720. [[CrossRef](#)]
28. Kim, B.; Park, Y.; Hong, D. Partial non-orthogonal multiple access (P-NOMA). *IEEE Wirel. Commun. Lett.* **2019**, *8*, 1377–1380. [[CrossRef](#)]
29. Deng, X.; Fan, W.; Cunha, T.E.B.; Ma, S.; Chen, C.; Dong, Y.; Zou, X.; Yan, L.; Linnartz, J.P.M.G. Two-dimensional power allocation for optical MIMO-OFDM systems over low-pass channels. *IEEE Trans. Veh. Technol.* **2022**, *71*, 7244–7257. [[CrossRef](#)]
30. Zeng, L.; O'Brien, D.C.; Le Minh, H.; Faulkner, G.E.; Lee, K.; Jung, D.; Oh, Y.; Won, E.T. High data rate multiple input multiple output (MIMO) optical wireless communications using white LED lighting. *IEEE J. Sel. Areas Commun.* **2009**, *27*, 1654–1662. [[CrossRef](#)]
31. Kahn, J.M.; Barry, J.R. Wireless infrared communications. *Proc. IEEE* **1997**, *85*, 265–298. [[CrossRef](#)]
32. Haas, H.; Yin, L.; Wang, Y.; Chen, C. What is LiFi? *J. Lightw. Technol.* **2016**, *34*, 1533–1544. [[CrossRef](#)]
33. Chen, C.; Zhong, X.; Fu, S.; Jian, X.; Liu, M.; Yang, H.; Alphones, A.; Fu, H.Y. OFDM-based generalized optical MIMO. *J. Light. Technol.* **2021**, *39*, 6063–6075. [[CrossRef](#)]

Disclaimer/Publisher's Note: The statements, opinions and data contained in all publications are solely those of the individual author(s) and contributor(s) and not of MDPI and/or the editor(s). MDPI and/or the editor(s) disclaim responsibility for any injury to people or property resulting from any ideas, methods, instructions or products referred to in the content.